Self-force in black hole scattering: a scalar-field toy model

Chris Whittall, Oliver Long & Leor Barack

Gravitational Self-Force and Scattering Amplitudes Workshop
University of Edinburgh
20th March 2024

Talk outline

A) Background: gravitational self-force and scattering

B) Scalar-field toy model

C) Frequency-domain numerical approach

D) Resumming PM results using SF

E) Large radius asymptotics of the SF

See also talk by O. Long after the coffee break

PART A: Background

The 2-body problem in GR: approaches

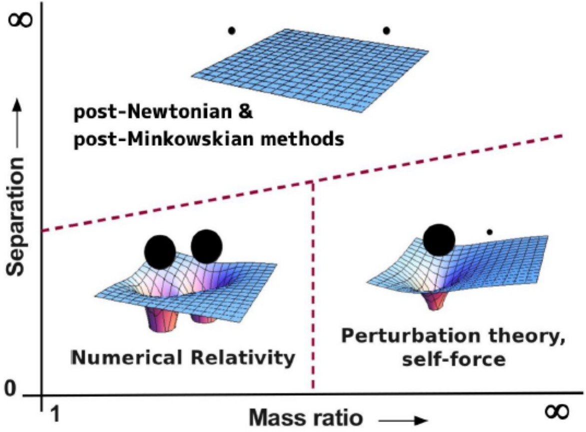

[Image credit: L. Barack & A. Pound]

Extreme mass ratio inspirals (EMRIs)

[Created using KerrGeodesics package from BHP toolkit.]

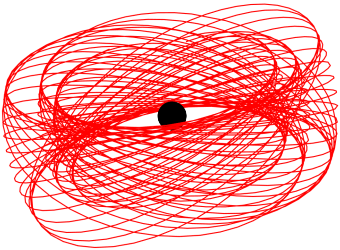

- Highly asymmetric compact binaries. Typical mass ratios

$$q \sim \frac{10 M_\odot}{10^6 M_\odot} = 10^{-5} \ll 1 \quad (1)$$

- Inspiral slow compared to orbital periods:

$$T_{\rm RR} \sim T_{\rm orb}/q \gg T_{\rm orb}. \quad (2)$$

- Large number of gravitational wavecycles in LISA band before merger:

$$N_{\rm orb} \sim 1/q \sim 10^5. \quad (3)$$

- Orbital dynamics complicated. Geodesics tri-periodic and generically ergodic.
- EMRIs offer a precision probe of strong-field geometry around black-holes.

Self-force expansion

Metric of the physical spacetime is expanded about background as a series in $q := m_1/m_2 \ll 1$,

$$g^{\mathrm{phys}}_{\alpha\beta} = g_{\alpha\beta} + q h^{(1)}_{\alpha\beta} + q^2 h^{(2)}_{\alpha\beta} + \ldots \tag{4}$$

- 0SF: Background metric $g_{\alpha\beta}$. Smaller object moves along fixed background geodesic.
- 1SF: Perturbation $h^{(1)}_{\alpha\beta}$ sourced by point particle on fixed background geodesic. Leading order conservative and dissipative self-forces $\propto q$.
- 2SF: Perturbation $h^{(2)}_{\alpha\beta}$ sourced by particle on 1SF-perturbed trajectory. Gives rise to additional self-force terms $\propto q^2$.

Particle description derived, not assumed.

1SF equation of motion

- Metric perturbation may be split into regular and singular fields, [Detweiler & Whiting 2003]

$$h_{\alpha\beta} = h^R + h^S, \tag{5}$$

defined in terms of certain acausal Green's functions.

- Only $h^R_{\alpha\beta}$ contributes to the self-force. For example, at 1SF order,

$$\frac{Du^\alpha}{d\tau} = q\nabla^{\alpha\beta\gamma} h^{R(1)}_{\beta\gamma}\Big|_{z(\tau)} + O(q^2), \tag{6}$$

where

$$\nabla^{\alpha\beta\gamma} h_{\gamma\beta} := -\frac{1}{2}\left(g^{\alpha\beta} + u^\alpha u^\beta\right) u^\gamma u^\delta \left(2\nabla_\delta h_{\beta\gamma} - \nabla_\beta h_{\gamma\delta}\right). \tag{7}$$

Computational approach: mode-sum regularisation

- Singular field subtracted mode-by-mode in a spherical harmonic expansion around the large BH:

$$F_{\rm self}(\tau) = m \sum_{\ell=0}^{\infty} \left[\left(\nabla h^{\rm ret}\right)^{\ell} - \left(\nabla h^{\rm S}\right)^{\ell} \right]_{z(\tau)} \tag{8}$$
$$= \sum_{\ell=0}^{\infty} \left[m \left(\nabla h^{\rm ret}\right)^{\ell} \Big|_{z(\tau)} - A(z)\ell - B(z) - C(z)/\ell \right] - D(z).$$

- Regularization parameters: derived analytically for generic Kerr orbits.

  [Barack & Ori 2000-03]

- Numerical input: modes of $h^{\rm ret}_{\alpha\beta}$ calculated numerically by solving perturbation equations with point-particle source and retarded BCs.

Scatter geodesics in Schwarzschild

Different parameterisations:

- Energy and angular momentum: $E > 1$ and $L > L_{\rm crit}(E)$
- Eccentricity and semi-latus rectum: e and $p > 6 + 2e$
- Velocity at infinity and impact parameter: $0 < v < 1$ and $b > b_{\rm crit}(v)$

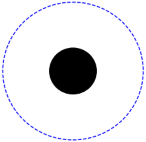

Why study scattering?

- Theoretical grounds:
  1. Can probe sub-ISCO region even at low velocities; down to light ring $r = 3M$ with large v.
  2. Scattering angle $\chi(b, v)$ defined unambiguously, even with radiation.

- Boundary-to-bound relations between scatter and bound orbit observables, derived using effective-field-theory. [Kalin & Porto 2020]

- $\chi_{\rm 1SF}$ determines **full** conservative dynamics to 4PM, valid at *any* mass ratio. Extend to 6PM with $\chi_{\rm 2SF}$ [Damour 2020]. PM expansion of χ can be used to calibrate effective-one-body models [Damour 2016].

- Can compare SF results with analytical PM for mutual validation; benchmark/calibrate PM in strong-field (see resummation).

PART B: Scalar-field toy model

Scalar-field toy model in Schwarzschild

- Toy model: scalar charge Q with mass m_1 moving in a background Schwarzschild spacetime of mass m_2:

$$\nabla^\mu \nabla_\mu \Phi = -4\pi Q \int_{-\infty}^{+\infty} \frac{\delta^4(x - x_p(\tau))}{\sqrt{-g(x)}} d\tau. \tag{9}$$

- Scalar-field calculation captures the main challenges of gravitational self-force calculations, in a simpler overall framework.

- Parameter $q_s := Q^2/(m_1 m_2) \ll 1$ takes the role of the mass ratio.

Scalar-field self-force

- Equation of motion: 4-momentum $m_1 u^\alpha$ evolves according to

$$\frac{D}{d\tau}(m_1 u^\alpha) = Q\nabla^\alpha \Phi^R. \tag{10}$$

- Component parallel to u^α controls mass variation:

$$\frac{dm_1}{d\tau} = -Q\frac{d\Phi^R}{d\tau} \implies m_1(\tau) = m_1^{\rm rest} - Q\Phi^R(\tau). \tag{11}$$

- Projection orthogonal to u^α defines the scalar-field self-force:

$$m_1\frac{Du^\alpha}{d\tau} = Q\left(\delta^\alpha_\beta + u^\alpha u_\beta\right)\nabla^\beta\Phi^R =: m_1 q_s F^\alpha. \tag{12}$$

Self-force correction to the scatter angle

- Scatter angle expanded as

$$\chi = \chi^{(0)} + q_s \delta\chi, \tag{13}$$

where $\chi^{(0)}$ is the scatter angle of the geodesic with the same (b, v).

- Correction expressed as integral over the worldline, [Barack & Long 2022]

$$\delta\chi = \int_{-\infty}^{+\infty} A_\alpha(\tau; b, v) F^\alpha(\tau) d\tau. \tag{14}$$

At $O(q)$, integral may be evaluated along limiting geodesic.

- Can split into conservative and dissipative pieces using orbital symmetries:

$$F_\alpha^{\rm cons}(r, \dot{r}_p) = -F_\alpha^{\rm cons}(r, -\dot{r}_p), \quad F_\alpha^{\rm diss}(r, \dot{r}_p) = F_\alpha^{\rm diss}(r, -\dot{r}_p) \quad (\alpha = t, \varphi). \tag{15}$$

Scalar-field self-force in terms of amplitudes

- Action:

$$S = \int d^D x \sqrt{-g} \left[-\frac{2}{\kappa^2} R + \frac{1}{2}\phi_1(\Box + m_1^2)\phi_1 + \frac{1}{2}\phi_2(\Box + m_2^2)\phi_2 + \frac{1}{2}\psi \Box \psi + \boxed{\frac{1}{2} Q \psi \phi_1^2} \right]$$

  $\phi_{1,2}$ black holes, scalar field ψ.

- 3-point vertices:

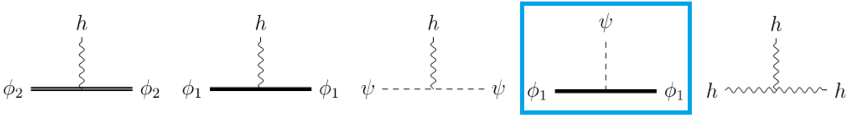

- Keep terms which are linear in mass-ratio and proportional to Q^2

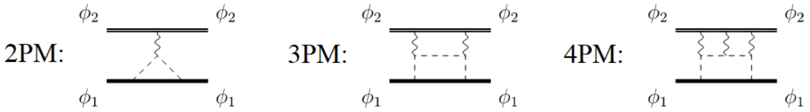

[Cheung, Rothstein, Solon] [Bern, Cheung, Roiban, Shen, Solon, Zeng]

[Bern, Cheung, Para-Martinez, Roiban, Ruf, Shen, Solon, Zeng]

PART C: Frequency domain numerical approach

Spherical harmonic decomposition

- Scalar field decomposed in basis of spherical harmonics,

$$\Phi = \frac{Q}{r} \sum_{\ell=0}^{\infty} \sum_{m=-\ell}^{+\ell} \psi_{\ell m}(t, r) Y_{\ell m}(\theta, \varphi). \tag{16}$$

- Field equation becomes:

$$-\frac{\partial^2 \psi_{\ell m}}{\partial t^2} + \frac{\partial^2 \psi_{\ell m}}{\partial r_*^2} + V_\ell(r)\psi = S(t, r)\delta(r - r_p(t)). \tag{17}$$

- Time-domain numerical treatment in [Barack & Long 2022] using double null coordinates and characteristic grid.

Frequency-domain methods

- Field equation reduced to ODEs using Fourier decomposition:

$$\psi_{\ell m}(t,r) = \int_{-\infty}^{+\infty} \psi_{\ell m\omega}(r) e^{-i\omega t}. \tag{18}$$

- Frequency-domain (FD) self-force methods highly valued for their accuracy and efficiency for bound orbits:
  - SF along generic bound geodesics in Kerr. [van de Meent 2018].

- FD methods expected to retain these advantages when moving to unbound orbits, but challenges must be overcome:
  - Continuous spectrum.
  - Failure of EHS method.
  - Slowly convergent radial integrals.
  - Cancellation during TD reconstruction.

Scalar-field toy model

- Field equation becomes

$$\frac{d^2\psi_{\ell m\omega}}{dr_*^2} - \left[V_\ell(r) - \omega^2\right]\psi_{\ell m\omega} = S_{\ell m\omega}(r). \tag{19}$$

- Admits homogeneous solutions $\psi^{\pm}_{\ell\omega}(r)$ obeying retarded BCs at either horizon or infinity. Retarded inhomogeneous solution constructed using variation of parameters:

$$\psi_{\ell m\omega}(r) = \psi^{+}_{\ell\omega}(r)\int_{r_{\rm min}}^{r}\frac{\psi^{-}_{\ell\omega}(r')S_{\ell m\omega}(r')}{W_{\ell\omega}f(r')}dr' + \psi^{-}_{\ell\omega}(r)\int_{r}^{+\infty}\frac{\psi^{+}_{\ell\omega}(r')S_{\ell m\omega}(r')}{W_{\ell\omega}f(r')}dr' \tag{20}$$

- Gibbs phenomenon: impractical to reconstruct SF modes from physical solution $\psi_{\ell m\omega}(r)$.

Extended homogeneous solutions [Barack, Ori & Sago 2008]

- Method of Extended Homogeneous Solutions restores exponential, uniform convergence.

VoP

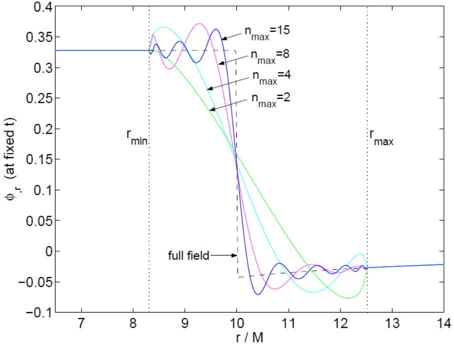

EHS

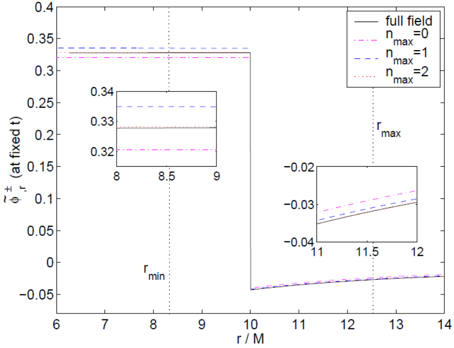

Extended homogeneous solutions: unbound orbits

- Physical time-domain field is reconstructed piecewise from **homogeneous** solutions.

- For example, SF modes in the "internal" region $r \leq r_p(t)$ reconstructed from

$$\tilde{\psi}^{-}_{\ell m\omega}(r) := C^{-}_{\ell m\omega}\psi^{-}_{\ell\omega}(r), \tag{21}$$

  where normalisation the factor $C^{-}_{\ell m\omega}$ is such that EHS and physical field coincide in $r \leq r_{\min}$.

- For unbound orbits, EHS cannot be used to reconstruct field in the "external" region $r > r_p(t)$.

  We use EHS and one-sided mode-sum regularisation

Truncation problem

- Normalisation factor $C^-_{\ell m\omega}$ can be expressed as an integral over the (unbounded) radial extent of the orbit:

$$C^-_{\ell m\omega} = \int_{r_{\min}}^{+\infty} \frac{\psi^+_{\ell\omega}(r')S_{\ell m\omega}(r')}{W_{\ell\omega}f(r')}dr'. \tag{22}$$

- Slow, oscillatory convergence: problems truncating at finite $r_{\max}$.

- Developed solutions:
  1. Tail corrections: use large-r approximation to integrand to derive analytical estimates to the neglected tail.
  2. Integration by parts (IBP): use IBP to increase decay rate of integrand.

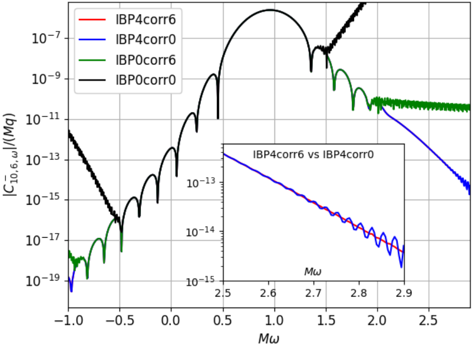

$C^-_{\ell m\omega}$ spectra

Example $C^-_{\ell m\omega}$ spectra for orbit $E = 1.1$, $r_{\min} = 4M$. Note QNM features.

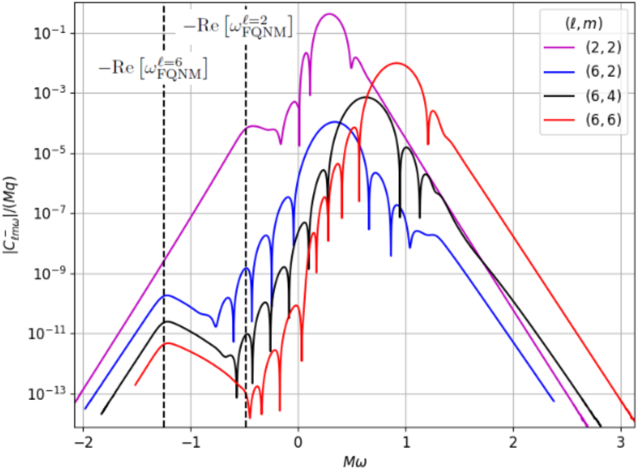

Self-force: regularisation tests

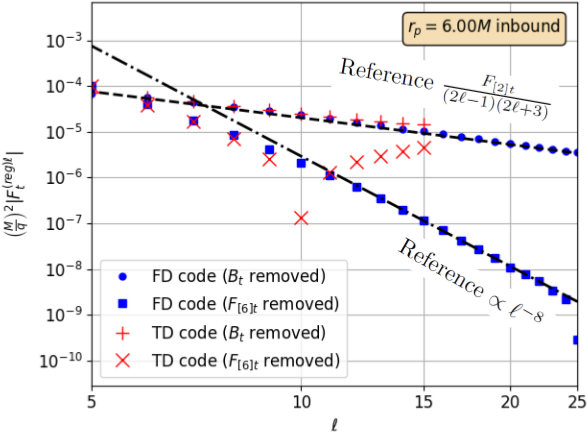

FD code agrees better with regularisation parameters at this radius

$$F(\tau) = \sum_{\ell=0}^{\infty} \left[q \left(\nabla \Phi^{\text{ret}}\right)^{\ell} \Big|_{z(\tau)} - A(z)\ell - B(z) - C(z)/\ell - H.O.P \right] - D(z)$$

Cancellation problem

- Significant cancellation between low-frequency modes at large ℓ and r.
- Caused by unphysical growth of the EHS field.
- Problem intrinsic to EHS approach. Afflicts scatter calculations more severely than bound orbit case.

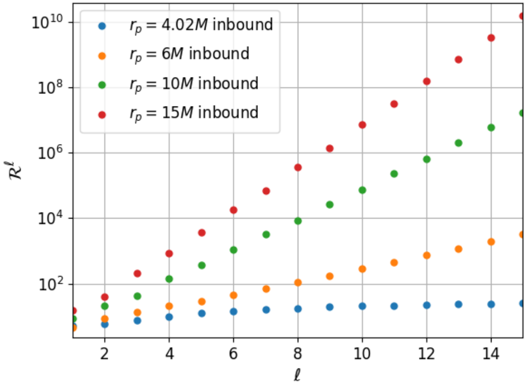

Partially mitigate using dynamic ℓ-truncation in the mode-sum.

Self-force: along orbit

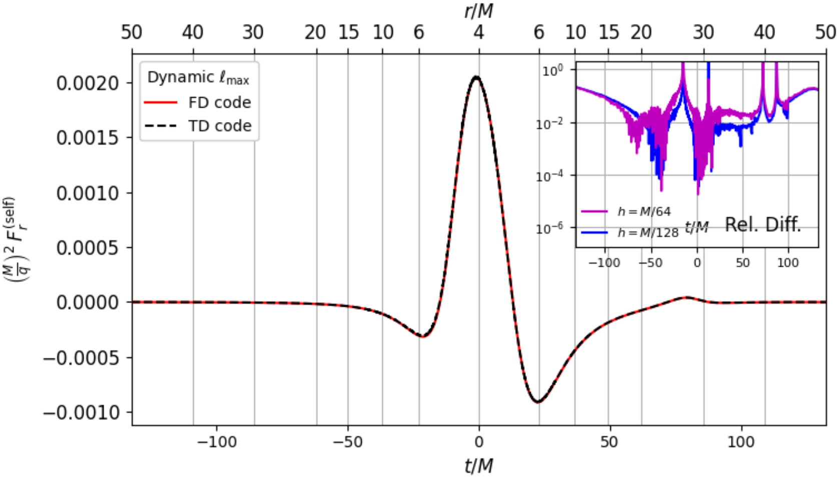

Gradual loss of accuracy along orbit due to progressive loss of ℓ-modes.

PART D: Resumming PM results using SF

Geodesic resummation

- As $b \to b_c(v)$, geodesic scatter angle diverges

$$\chi_{0\mathrm{SF}} \sim A(v) \log\left(1 - \frac{b_c(v)}{v}\right) + const(v) + \dots \tag{23}$$

- Resum PM results using singularity structure, similar to [Damour & Rettegno 2023]. Introduce

$$\Psi^{\mathrm{nPM}}_{0\mathrm{SF}}(b, v) := A(v) \left[\log\left(1 - \frac{b_c(v)}{b}\right) + \sum_{k=1}^{n} \frac{1}{k} \left(\frac{b_c(v)}{b}\right)^k\right]. \tag{24}$$

- Resummed scattering angle

$$\tilde{\chi}^{\mathrm{nPM}}_{0\mathrm{SF}}(b, v) = \chi^{\mathrm{nPN}}_{0\mathrm{SF}}(b, v) + \Psi^{\mathrm{nPM}}_{0\mathrm{SF}}(b, v). \tag{25}$$

  Matches nPM result in $b \to \infty$ limit, logarithmic divergence of $\chi_{0\mathrm{SF}}$ as $b \to b_c(v)$.

Geodesic resummation: results

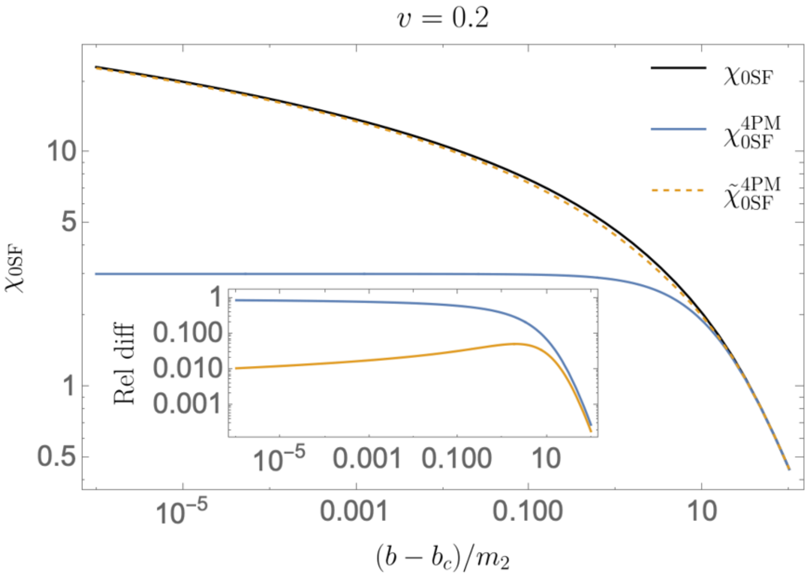

$\delta\chi_{1\mathrm{SF}}$ near the transition to plunge

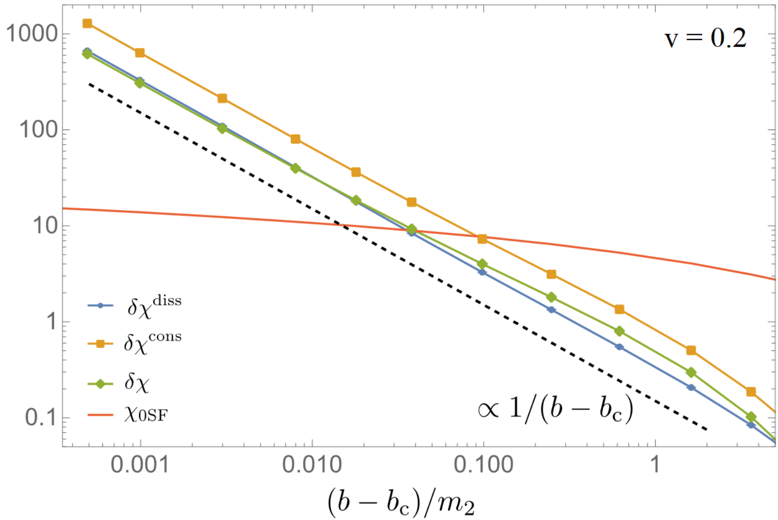

Find $\delta\chi_{1\mathrm{SF}} \sim 1/(b - b_c(v))$ as $b \to b_c(v)$.

1SF resummation

- Divergence

$$\delta\chi_{1SF} \sim q_s B(v) \frac{b_c(v)}{b - b_c(v)} \text{ as } b \to b_c(v). \tag{26}$$

- Introduce

$$\Psi^{\mathrm{nPM}}(b, v) := A \left[\log\left(1 - \frac{b_c(v)(1 - q_s B/A)}{b}\right) + \sum_{k=1}^{n} \frac{1}{k} \left(\frac{b_c(v)(1 - q_s B/A)}{b}\right)^k \right]. \tag{27}$$

- 1SF-resummed scatter angle

$$\tilde{\chi}^{\mathrm{nPM}}(b, v) := \chi^{\mathrm{nPM}}(b, v) + \Psi^{\mathrm{nPM}}(b, v). \tag{28}$$

  Matches *nPM* result in $b \to \infty$ limit, and 0SF and 1SF divergences as $b \to b_c(v)$.

- Coefficient $B(v)$ extracted numerically.

1SF resummation: results (preliminary)

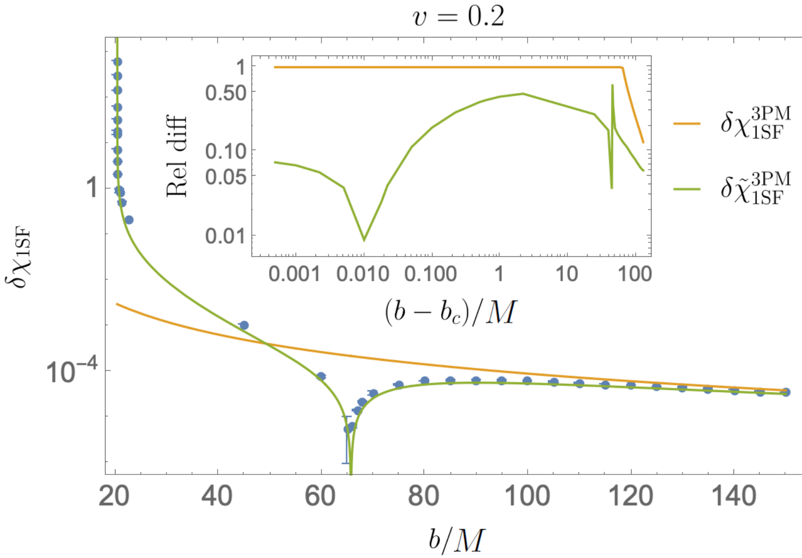

1SF resummation: results (preliminary)

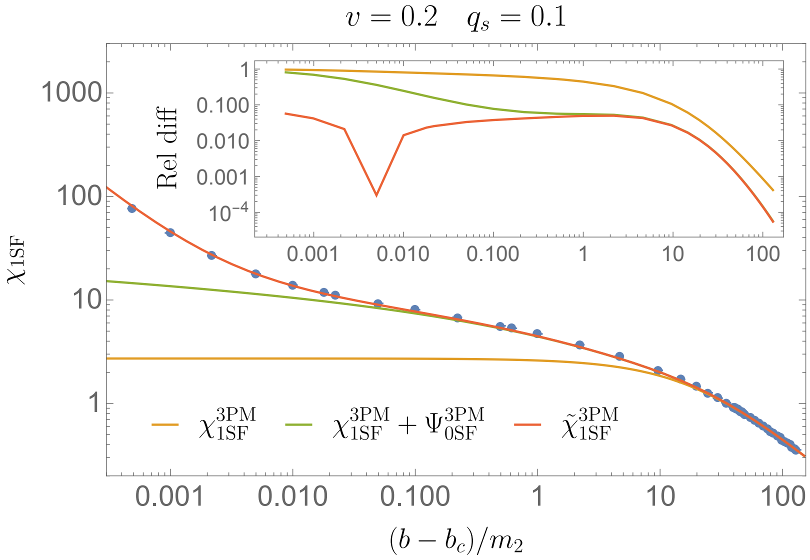

Improvement compared to geodesic resummation.

PM resummation: additional developments (preliminary)

- **High velocities:** large-ℓ modes become more important at higher velocities.
  - Possibly related to relativistic beaming of radiation.
  - Effect strongest near periapsis.
  - FD code can get $\ell \geq 15$ modes near periapsis.
  - Developing FD/TD hybrid method.

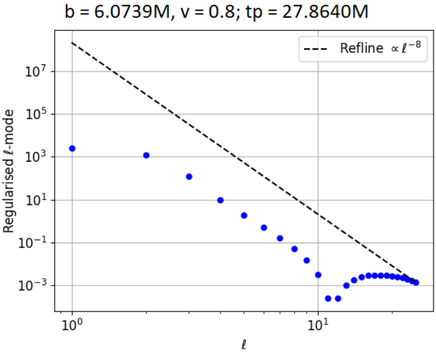

- **Direct approach**: express $B(v)$ as integral over critical orbit, $b = b_c(v)$.
  - Only need to calculate SF along critical orbit. More accurate and efficient than fitting.
  - Numerical methods need some modification e.g. for FD must handle distributional piece of spectrum arising from asymptotic circular orbit.

PART E: Large radius asymptotics of the SF

Analytical calculation: overview

- Want analytical expressions for scalar-field/self-force as $t \to \pm\infty$ as an expansion in $1/r_p$:
  1. Supplement FD code at large radii.
  2. Supplement TD codes, evolve over shorter periods.
  3. Provide initial conditions to TD evolutions, reducing junk radiation.
  4. Large-r tails in scatter angle integrals.
- Makes use of a hierarchical expansion introduced in [Barack 1999],

$$\psi_{\ell m}(u, v) = \sum_{n=0}^{\infty} \psi_n(u, v),$$

$$\psi_{0,uv} + V_0(\ell; r)\psi_0 = S_{\ell m}(u)\delta(v - v_p(u)),$$

$$\psi_{n,uv} + V_0(\ell; r)\psi_n = -\delta V(\ell; r)\psi_{n-1} \quad (n \geq 1),$$

$$V_0(\ell > 0; r_* < R) := 0; \quad V_0(\ell > 0; r_* \geq R) := \frac{\ell(\ell+1)}{4r_*^2}; \quad V_0(\ell = 0; r) = \delta(R)/M,$$

$\delta V(\ell; r) = V(\ell; r) - V_0(\ell; r)$ and $-\infty \ll R \ll r_{\min *}$ is some cut-off.

Analytical calculation: ψ_0 order (preliminary)

$$\psi_0(u,v) = \int_{-\infty}^{u} du' \int_{-\infty}^{v} dv' \; G(u,v;u',v') S(u') \delta(v' - v_p(u')) \tag{29}$$

- Leading order piece $\sim 1/r_p^2$:
  - Calculation complete.
  - Does not contribute to SF (confirmed analytically).
  - Initial comparisons to numerical data promising.

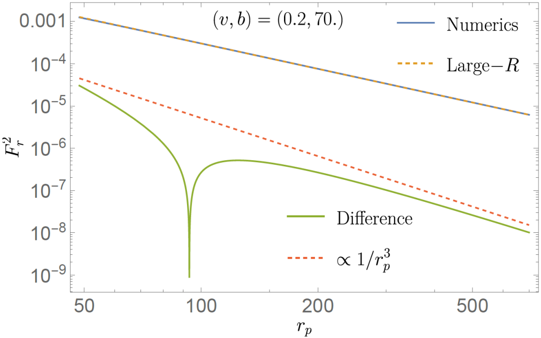

- Next-to-leading order piece $\sim 1/r_p^3$:
  - Calculation incomplete.
  - Expect NLO orbit terms to contribute to the leading-order SF.

Analytical calculation: ψ_1 order (preliminary)

Multiple integration with 2 Green's functions:

$$\psi_1(x) = -\int_{-\infty}^{u} du' \int_{-\infty}^{v} dv' \; G(x;x')\delta V(r')\psi_0(x') \tag{30}$$
$$= -\int_{-\infty}^{\tilde{u}(u,v)} du'' \int_{u''}^{u} du' \int_{v_p(u'')}^{u} dv' \; G(x;x'), \delta V(r')G(x';u'',v_p(u''))S(u'')$$

where $x := (u,v)$ etc., $\tilde{u} = u$ for $v \geq v_p(u)$ and $\tilde{u} = u_p(v)$ for $v < v_p(u)$.

- Leading order piece $\sim 1/r_p^3$:
  - Contributes to leading-order SF.
  - Integral divided into many sections - many do not contribute.
  - Calculation ongoing.

Summary

- Scattering is now a well-established application of SF. SF complements other available approaches.
- Scalar-field toy model used extensively for method development.
- Time and frequency domain numerical approaches available. FD more accurate in strong field, but deteriorates further away.
- SF data may be used to resum PM results, extending validity of the latter.
- Numerical SF calculations may be complemented and improved by analytical results for the SF at early/late time.